Hadronic rapidity spectra in heavy ion collisions at SPS and AGS energies in a quark combination model*

SUN Le-Xue(孙乐学)[1] WANG Rui-Qin(王瑞芹)[2]
SONG Jun(宋军)[2] SHAO Feng-Lan(邵凤兰)[1;1)]

[1] Department of Physics, Qufu Normal University, Shandong 273165, China
[2] Department of Physics, Shandong University, Shandong 250100, China

Abstract: The quark combination mechanism of hadron production is applied to nucleus-nucleus collisions at the CERN Super Proton Synchrotron (SPS) and the BNL Alternating Gradient Synchrotron (AGS). The rapidity spectra of identified hadrons and their spectrum widths are studied. The data of π^-, $K^{\pm}$, ϕ, Λ, $\overline{\Lambda}$, Ξ^- and $\overline{\Xi}^+$ at 80 and 40 A GeV, and in particular at 30 and 20 A GeV where the onset of deconfinement is suggested to happen, are consistently described by the quark combination model. However, at AGS 11.6 A GeV below the onset, the $\pi^{\pm}$, $K^{\pm}$ and Λ spectra cannot be simultaneously explained, indicating the disappearance of the intrinsic correlation of their production in the constituent quark level. The collision-energy dependence of the rapidity spectrum widths of the constituent quarks, and the strangeness of the hot and dense quark matter produced in heavy ion collisions, are obtained and discussed.

Key words: relativistic heavy ion collisions, rapidity spectra, quark combination

PACS: 25.75.Dw, 25.75.Nq, 25.75.-q **DOI:** 10.1088/1674-1137/36/1/009

1 Introduction

The production of quark gluon plasma (QGP) and its properties are hot topics in relativistic heavy ion collisions. A huge number of possible QGP signals have been proposed and measured, and many unexpected novel phenomena have been observed at the RHIC and the Super Proton Synchrotron (SPS) [1–5]. These experimental data greatly contribute to the identification of QGP and the understanding of its properties and hadronization from different aspects. In particular, there is a class of phenomena that are of particular interest, i.e. the abnormally high ratio of baryons to mesons and the quark number scaling of hadron elliptic flows in the intermediate $p_{\rm T}$ range, etc. [6, 7]. These phenomena reveal the novel features of hadron production in relativistic heavy ion collisions.

In a quark combination/coalescence scenario, hadrons are combined from quarks and antiquarks, i.e. a quark-antiquark pair merges into a meson and three quarks into a baryon. The production difference between baryons and mesons mainly results from their different constituent quark numbers. It is shown that such simple quark number counting can naturally explain the striking features of hadron production observed at RHIC [8–10], while the fragmentation mechanism cannot.

The highlights at RHIC are mainly of hadron production in a transverse direction, where the quark combination scenario mostly flashes. In fact, the longitudinal rapidity distribution of hadrons is also a good tool for testing the hadronization mechanism. In previous work [11, 12], we used the quark combination model to successfully describe the rapidity spectra of various hadrons at RHIC $\sqrt{s_{\rm NN}}=200$ GeV and top SPS $E_{\rm beam}=158$ A GeV. At other collision energies where the QGP may be produced, e.g. at lower SPS and higher LHC energies, does the quark combination mechanism still work well? The beam

Received 3 May 2011
* Supported by National Natural Science Foundation of China (11175104, 10947007, 10975092)
1) E-mail: shaofl@mail.sdu.edu.cn

energy scan at RHIC and the NA49 collaboration have provided abundant data on hadron production in the energy region from 20 to 6 GeV. In this paper, we extend the quark combination model to systematically study the rapidity distributions of various identified hadrons in heavy ion collisions at SPS, $E_{\rm beam} = 80,\ 40,\ 30,\ 20\ A$ GeV, and the Alternating Gradient Synchrotron (AGS), $E_{\rm beam} = 11.6\ A$ GeV, and test the applicability of the quark combination mechanism.

2 A brief introduction to the quark combination model

The quark combination model deals with how quarks and antiquarks convert to color-singlet hadrons as the partonic matter evolves to the interface of hadronization. The basic idea is to make all the quarks and antiquarks line up in a one-dimensional order in phase space, e.g. in rapidity, and let them combine into hadrons one by one, following a combination rule based on the QCD and near-correlation in the phase space requirements. See Section 2 of Ref. [12] for a detailed description of such a rule. Here, we consider only the production of $SU(3)$ ground states, i.e. 36 plets of mesons and 56 plets of baryons. The flavor $SU(3)$ symmetry with strangeness suppression in the yields of initially produced hadrons is fulfilled in the model. The decay of short-life hadrons is systematically taken into account to make the spectra comparable to the data. The model has reproduced the experimental data for hadron multiplicity ratios, momentum distributions and the elliptic flows of identified hadrons, for example in heavy ion collisions at RHIC and top SPS energies [12–16], and addressed the entropy issue [17] and exotic state production [18].

3 The rapidity spectra of constituent quarks

The rapidity spectra of constituent quarks just before hadronization are needed as the input of the quark combination model. Considering the collision energies studied here are much lower than RHIC energies, and in particular 30–20 A GeV is the possible region for the onset of deconfinement, it is not certain whether the hot and dense quark matter is produced exactly at these energies, so applying a model or theory for the evolution of the hot and dense quark matter, e.g. relativistic hydrodynamics, to get the quark spectra before hadronization may be uneconomic or infeasible. In this paper, assuming the hot quark matter has been created, we parameterize the rapidity distribution of constituent quarks and extract the parameter values from the experimental data of final state hadrons. The rapidity distribution of newborn quarks is taken to be a Gaussian-like form, i.e.

$$\frac{{\rm d}N_{\rm q}}{{\rm d}y} = N_{\rm q} f_{\rm q}(y) = \frac{N_{\rm q}}{A}\left({\rm e}^{-|y|^a/2\sigma^2} - C\right). \qquad (1)$$

Here, $C = \exp[-|y_{\rm beam}|^a/2\sigma^2]$, which means that the constituent quarks that form hadrons via combination are within $[-y_{\rm beam},\ y_{\rm beam}]$ in the center-of-mass frame. A is the normalization factor, satisfying

$$A = \int_{-y_{\rm beam}}^{y_{\rm beam}} \left({\rm e}^{-|y|^a/2\sigma^2} - C\right){\rm d}y.$$

a and σ are the parameters depicting the shape of the spectrum. $N_{\rm q}$ denotes the total number of newborn quarks with type q in the full rapidity region. For the net quarks coming from the colliding nuclei, their evolution is generally different from the newborn quarks due to the complicated collision transparency [19]. We fix the rapidity spectrum of net quarks before hadronization using the data of the rapidity distribution of net protons [20], and the results are shown in Fig. 1.

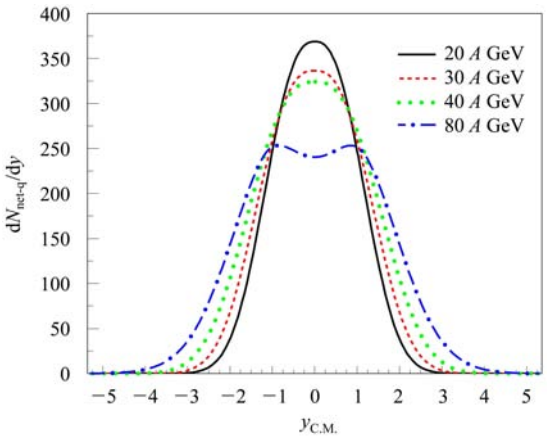

Fig. 1. The rapidity distributions of net quarks.

4 Hadronic rapidity spectra at SPS and AGS

In this section, we first use the quark combination model to systematically study the hadron rapidity spectra and their widths at SPS energies. Then we present the energy dependence of the strangeness and spectrum width of constituent quarks. Finally, we show the results at AGS 11.6 A GeV.

4.1 Rapidity spectra of hadrons at SPS energies

The calculated rapidity distributions of identified hadrons in central Pb+Pb collisions at $E_{\rm beam} = 80$, 40, 30 and 20 A GeV are shown in Fig. 2. The values of the parameters for newborn quarks are listed in Table 1, and χ^2/ndf is presented as the quality of global fitting. Note that the experimental data of pions beyond $y_{\rm beam}$ are not included in the χ^2/ndf calculation because the limiting fragmentation behavior around $y_{\rm beam}$ becomes prominent, which is beyond the study of this paper by quark combination. The results show that the quark combination model can reproduce the experimental data of various identified hadrons except ϕ at 30, 20 A GeV. The yields of ϕ at 30 and 20 A GeV deviate from the data, but their sharps are still in agreement with the data after scaling by proper constant factors.

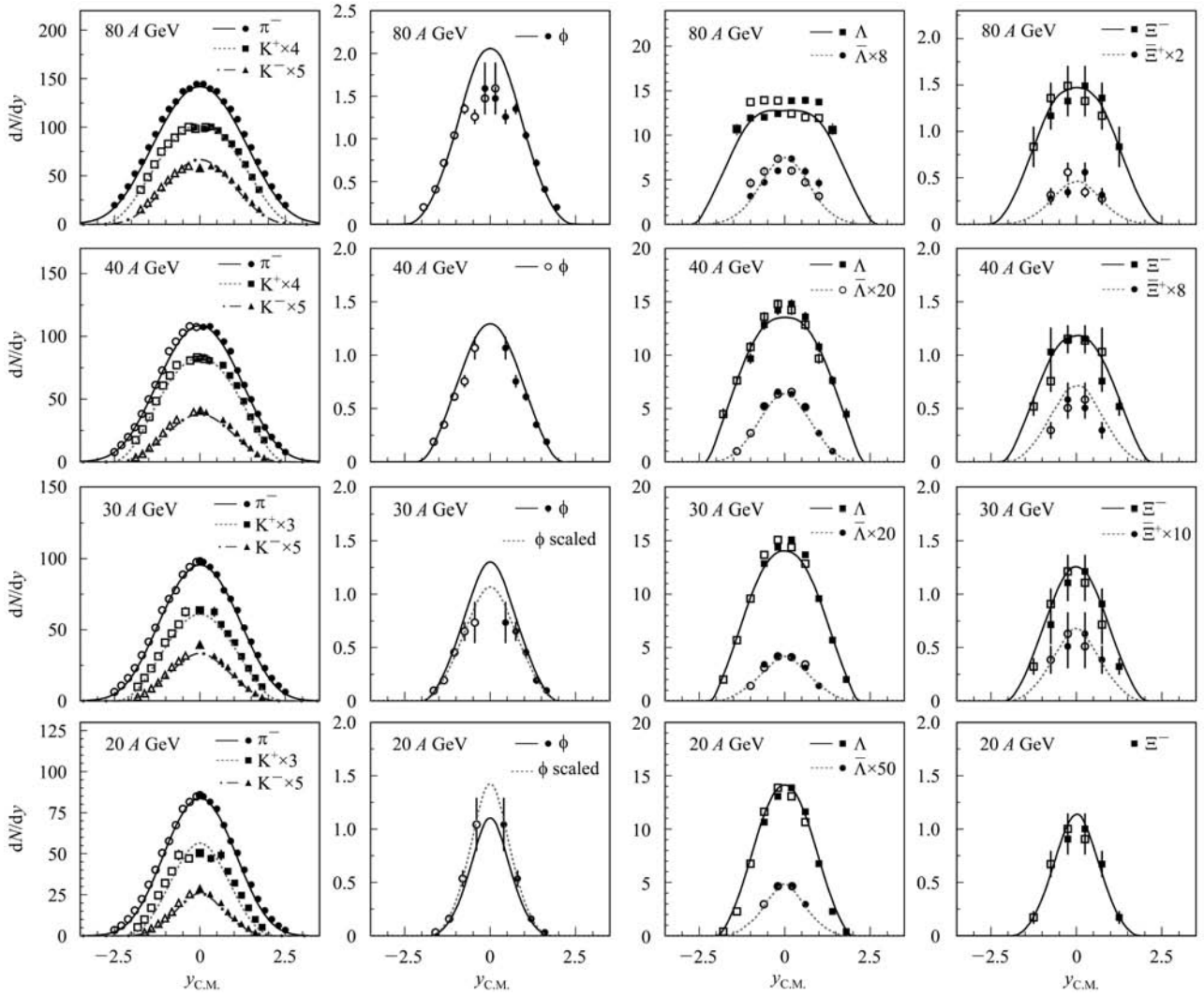

Fig. 2. Rapidity distributions of identified hadrons in central Pb+Pb collisions at $E_{\rm beam}$=80, 40, 30 and 20 A GeV. The symbols are the experimental data [21–25] and the lines are the calculated results. The open symbols are the reflection of measured data (solid symbols) against mid-rapidity. The results of ϕ at 30 and 20 A GeV are scaled by proper constant factors for comparing their shapes with the data.

Table 1. Parameters of newborn light, strange quarks and χ^2/ndf.

energy	$a_{\rm u/d}$	$a_{\rm s}$	$\sigma_{\rm u/d}$	$\sigma_{\rm s}$	$N_{\rm u/d}$	$N_{\rm s}$	χ^2/ndf
80 A GeV	1.90	2.35	1.19	1.40	275.2	159.6	0.98
40 A GeV	1.90	2.25	1.12	1.40	171.3	116.5	1.01
30 A GeV	1.80	2.05	1.20	1.16	139.0	101.5	0.96
20 A GeV	1.80	1.95	1.10	0.85	105.5	77.0	1.90

The deviation of ϕ yields at 30 and 20 A GeV is related to the pronounced rescattering effect. It is shown that at higher SPS and RHIC energies the production of ϕ mainly comes from the contribution of the partonic phase, i.e. the directly produced ϕ by hadronization, while at lower SPS energies kaon coalescence may be the dominated production mechanism [25]. In addition, the directly produced ϕ after hadronization will possibly suffer destruction by the scattering of the daughter kaons with other produced hadrons. The absence of these two effects at the hadronic stage in our calculations is the main reason for the deviation in ϕ yields.

4.2 The widths of the rapidity spectra for hadrons

From the above experimental data, one can see that the widths of the rapidity spectra for different hadron species are generally different. This difference, in other words the correlation of longitudinal hadron production, can be used to quantitatively test various hadronization models. In the quark combination mechanism, the rapidity distribution of a specific hadron is the convolution of the rapidity spectra of its constituent quarks and combination probability function (denoted by the combination rule in our model). Since the rapidity distributions of different-flavor quarks are different (see Table 1 and Fig. 1), in particular the difference between newborn quarks and net quarks, the shapes of the rapidity spectra of hadrons with different quark flavor components are generally different and correlated with each other by constituent quarks. Here, we calculate the spectrum widths of various hadrons to clarify this feature.

Considering that the rapidity regions covered by the data for different hadron species or at different collision energies are not the same, we define the variance of rapidity distribution for a specified hadron in a finite rapidity region limited by the discrete experimental data,

$$\langle y^2\rangle^{(\mathrm{L})} = \frac{\sum\limits_{i=1}^{n} y_i^2 \dfrac{\mathrm{d}N_i}{\mathrm{d}y}}{\sum\limits_{i=1}^{n} \dfrac{\mathrm{d}N_i}{\mathrm{d}y}}. \tag{2}$$

Here n is the number of experimental data, and y_i and $\mathrm{d}N_i/\mathrm{d}y$ are the rapidity position and corresponding yield density measured experimentally, respectively. Replacing $\mathrm{d}N_i/\mathrm{d}y$ with the model results, we can give the $\langle y^2\rangle^{(\mathrm{L})}|_{\mathrm{model}}$ and compare it with the experimental value $\langle y^2\rangle^{(\mathrm{L})}|_{\mathrm{data}}$ to test the applicability of the model without any arbitrariness caused by the rapidity regions where the experimental data have not yet covered. We further extrapolate $\langle y^2\rangle^{(\mathrm{L})}|_{\mathrm{data}}$ to the full rapidity region $[-y_{\mathrm{beam}}, y_{\mathrm{beam}}]$ via the relation

$$\langle y^2\rangle^{(\mathrm{F})}|_{\mathrm{data}} = \frac{\langle y^2\rangle^{(\mathrm{L})}|_{\mathrm{data}}}{\langle y^2\rangle^{(\mathrm{L})}|_{\mathrm{model}}} \langle y^2\rangle^{(\mathrm{F})}|_{\mathrm{model}}, \tag{3}$$

where $\langle y^2\rangle^{(\mathrm{F})}|_{\mathrm{model}}$ is the variance calculated by the model in the full rapidity region. The degree of agreement between $\langle y^2\rangle^{(\mathrm{F})}|_{\mathrm{model}}$ and the experimental data $\langle y^2\rangle^{(\mathrm{F})}|_{\mathrm{data}}$ still represents the original description ability of the model, and the $\langle y^2\rangle$ of different hadron species can be directly compared and their energy dependence is recovered. The spectrum widths of various hadrons, i.e. $D(y)^{(\mathrm{F})} \equiv \sqrt{\langle y^2\rangle^{(\mathrm{F})}}$, are calculated and the results are shown in Fig. 3 (158 A GeV is also included). One can see that the $D(y)$ of various hadrons given by the model are obviously distinguished. The agreement between the data and the calculated results is the support of the theoretic (quark recombination mechanism) explanation for the widths of hadronic rapidity distributions.

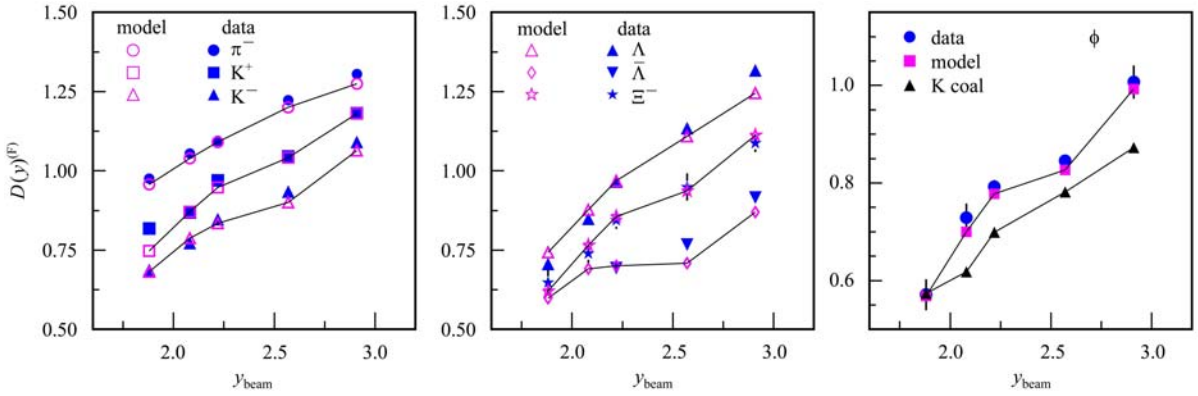

Fig. 3. Widths of rapidity distributions $D(y)^{(\mathrm{F})}$ at $E_{\mathrm{beam}}(y_{\mathrm{beam}})$=158, 80, 40, 30, 20 A GeV (2.91, 2.57, 2.22, 2.08, 1.88). The right panel includes the results of $\mathrm{K}^+\mathrm{K}^-$ coalescence for ϕ production. The model results are connected by the solid lines to guide the eye.

As stated above, at lower SPS energies kaon meson coalescence may be an important mechanism for ϕ production. The right panel of Fig. 3 shows the ϕ's $D(y)^{(\mathrm{F})}|_{\mathrm{data}}$ and $D(y)^{(\mathrm{F})}|_{\mathrm{model}}$ as well as the results for $\mathrm{K^+K^-}$ coalescence $D(y)^{(\mathrm{F})}|_{\mathrm{coal}}$. Similar to Ref. [25], considering the ideal case of the coalescence of two kaons with the same rapidity, we use the measured kaon rapidity distributions $f_{\mathrm{K}^\pm}(y)$ to obtain the spectrum of ϕ by $f_\phi^{\mathrm{coal}}(y) \propto f_{\mathrm{K}^+}(y) f_{\mathrm{K}^-}(y)$ and then give the $D(y)^{(\mathrm{F})}|_{\mathrm{coal}}$. One can see that at collision energies above 20 A GeV, $D(y)^{(\mathrm{F})}|_{\mathrm{coal}}$ is much smaller than the data, which is similar to the results in Ref. [25], while our results nearly agree with the data. This clearly shows that the ϕ production at these energies is dominated by the hadronization. At 20 A GeV, $D(y)^{(\mathrm{F})}|_{\mathrm{coal}}$ is nearly equal to the data and the model result is also in agreement with the data. This suggests that ϕ production at the lowest SPS energy can have different explanations, in other words, even though kaon coalescence is significant, the ϕ directly produced from hadronization may be ineligible.

4.3 The strangeness and spectrum width of constituent quarks

Let us turn to the extracted rapidity distributions of newborn light and strange quarks. Their properties can be characterized by two quantities, i.e the ratio of strange quark number N_{s} to light quark number $N_{\mathrm{u/d}}$, called the strangeness suppression factor λ_{s}, and the width of the rapidity spectrum.

The top panel of Fig. 4 shows the strangeness suppression factor λ_{s} at different collision energies. Note that λ_{s} defined here is in terms of quark numbers in the full phase space, so the values are sightly different from those in terms of the mid-rapidity quark number densities in the previous Ref. [12]. As the comparison with SPS, we also present λ_{s} at RHIC $\sqrt{s_{\mathrm{NN}}} = 200$, 62.4 GeV calculated by the model and at AGS 11.6 A GeV calculated by counting the numbers of light and strange valance quarks hidden in the observed pions, kaons and Λ, which are mostly abundant hadron species carrying light and strange gradients of the system. One can see that the value of λ_{s} exhibits a peak behavior at lower SPS energies. This behavior has been reported by the NA49 Collaboration as the signal of onset of deconfinement [5].

The width of rapidity spectrum is characterized by $D(y) \equiv \sqrt{\langle y^2\rangle - \langle y\rangle^2} = \sqrt{\langle y^2\rangle}$. The bottom panel of Fig. 4 shows the $D(y)$ of newborn light and strange quarks at different collision energies. The results at RHIC $\sqrt{s_{\mathrm{NN}}} = 200$, 62.4 GeV and SPS $E_{\mathrm{beam}} =$ 158 A GeV are included. One can see that with the increasing collision energy, $D(y)$ of newborn light and strange quarks both increase regularly, indicating the stronger collective flow formed at higher energies. As collision energy is equal to or greater than 40 A GeV, $D(y)$ of newborn light quarks are always smaller than those of the strange quarks, while at 30 and 20 A GeV the situation flips. The wider spectrum of strange quarks, relative to light quarks, has been verified at RHIC both in the longitudinal and transverse directions [12, 16, 26], and the explanation is that strange quarks acquire stronger collective flow during evolution in the partonic phase. As the collision energy reduces to 30 and 20 A GeV, the widths of the rapidity distributions of light and strange quarks, see Table 1 and Fig. 4, are all quite narrow, which means that the collective flow formed in the partonic phase is much smaller than those at higher SPS and RHIC energies. Therefore, the partonic bulk matter, even if produced as indicated by our results via still active constituent quark degrees of freedom, should be in the vicinity

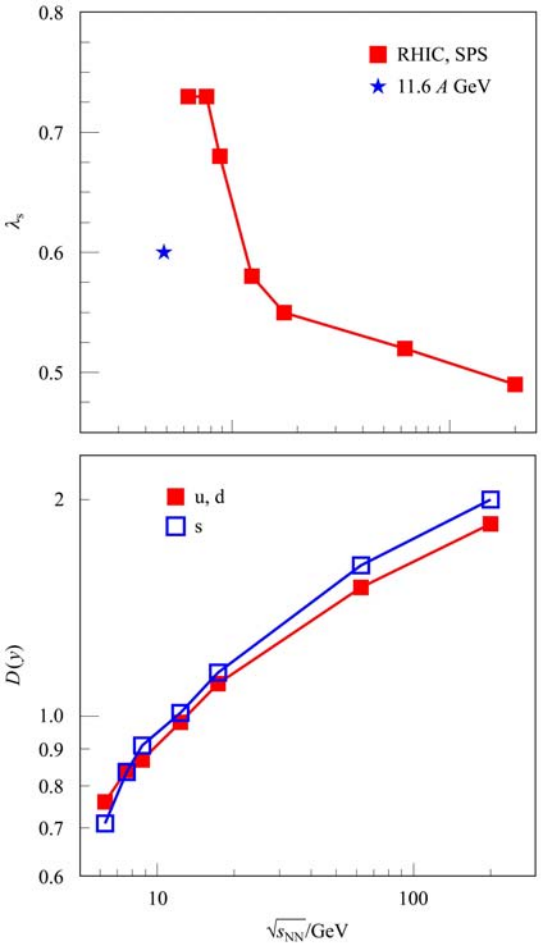

Fig. 4. The strangeness suppression factor λ_{s} and $D(y)$ of newborn light and strange quarks at different collision energies. The results are connected by the solid lines to guide the eye.

of phase boundary, and the extracted momentum distributions of quarks keep the memory of their original excitation. If thermal equilibrium is reached in heavy ion collisions, the quark occupation function in momentum space follows as $\exp[-E/T] = \exp[-m_{\rm T}\cosh(y)/T]$ in the case of no collective flow. Taking the hadronization temperature $T = 165$ MeV and constituent mass $m_{\rm q} = 340$ MeV for light quarks and $m_{\rm s} = 500$ MeV for strange quarks, the quark rapidity spectrum is of Gaussian form and the width of light quarks is $\sigma_{\rm q} = 0.6$ and strange quarks $\sigma_{\rm s} = 0.52$ due to the heavier mass. The tighter spread of strange quarks in rapidity space can be qualitatively understood in quark production with thermal-like excitation.

4.4 Results at AGS 11.6 *A* GeV

What happens at lower AGS energies? We further use the model to calculate the rapidity distributions of various hadrons at 11.6 *A* GeV. The results are shown in Fig. 5 and are compared with the experimental data. The values of parameters (a, σ, $N_{\rm q}$) for quark spectra are taken to be (2.1, 0.88, 71) for newborn light quarks and (2.0, 0.83, 42) for strange quarks, respectively. The rapidity distribution of net quarks is extracted from the proton data of the E802 Collaboration [28, 30], and the data of the E877 Collaboration [27] at 10.8 *A* GeV are used as the extrapolation guide of the net-quark spectrum in the forward rapidity region. One can see that the results for pions and kaons are in agreement with the data, but the result of Λ cannot reproduce the experimental data – the spectrum width given by the model is much wider than that of the data. This suggests that there is no intrinsic correlation at constituent quark level between the production of kaons and Λ at AGS 11.6 *A* GeV. In addition, the rapidity distributions of ϕ, K^0_s, $\overline{p}$, $\overline{\Lambda}$ and $\Xi^-(\overline{\Xi}^+)$ are predicted to be tested by future data.

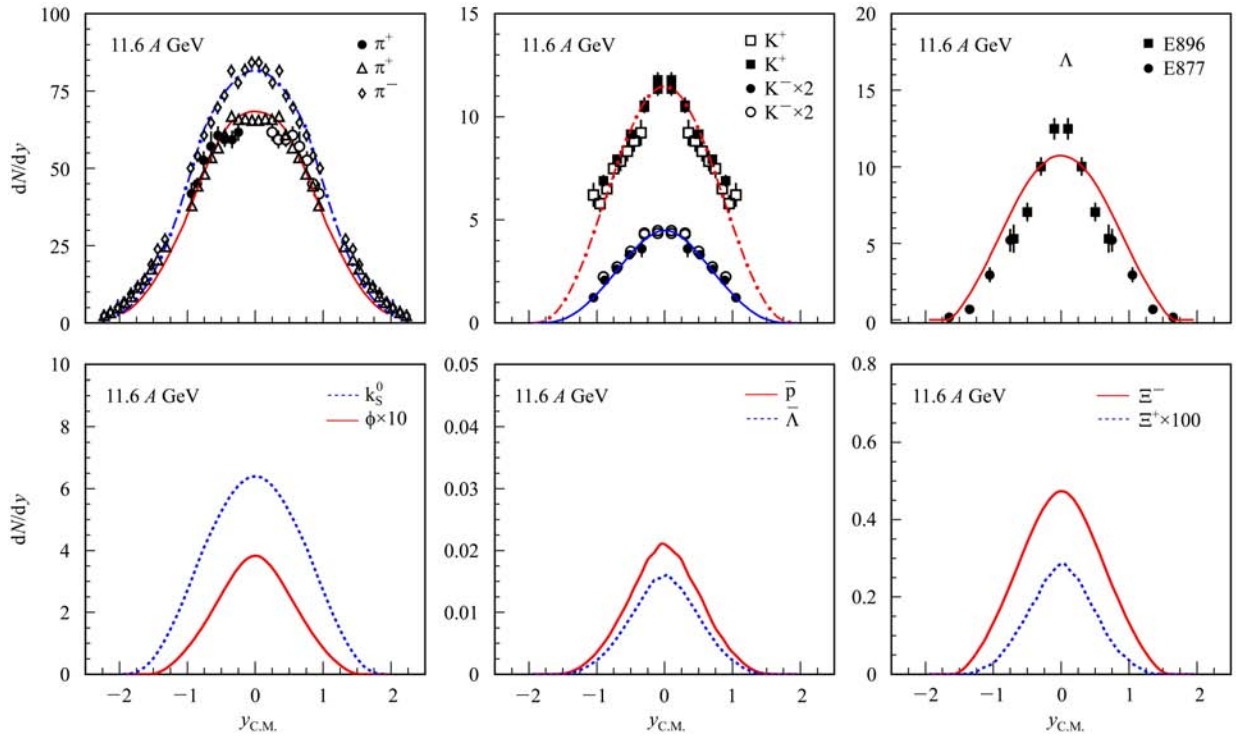

Fig. 5. Rapidity distributions of identified hadrons in central Au+Au collisions at $E_{\rm beam}$ =11.6 *A* GeV. The symbols are experimental data from Refs. [27–32] and the lines are the calculated results.

5 Summary

In this paper we have investigated, with the quark combination model, the rapidity distributions of identified hadrons and their widths in central A+A collisions at SPS and AGS energies. Assuming in advance the existence of constituent quark degrees of freedom, we parameterize the rapidity spectra of quarks before hadronization, then test whether such a set of light and strange quark spectra can self-consistently explain the data of π^-, $K^{\pm}$, ϕ, $\Lambda(\overline{\Lambda})$, $\Xi^-(\overline{\Xi}^+)$, etc. at these energies. The results of hadronic rapidity

spectra are in agreement with the data at 80 and 40 A GeV. At 30 and 20 A GeV, where the onset of deconfinement is suggested to happen, the model can still basically describe the production of various hadrons. The study of rapidity-spectrum widths for hadrons, particularly for the phi meson via comparison with the results from kaon coalescence in the hadronic rescattering stage, clearly show that hadron production at collision energies above 20 A GeV is dominated by hadronization. The energy dependence of the rapidity-spectrum widths of constituent quarks and the strangeness of the hot and dense quark matter are obtained. It is shown that strangeness peaks around 30 A GeV and below (above) the energy, the width of the strange quarks becomes smaller (greater) than that of the light quarks. As the collision energy decreases to AGS 11.6 A GeV, it is found that the production of $\pi^{\pm}$, $K^{\pm}$ and Λ cannot be consistently explained by the model, which suggests that there seems to be no intrinsic correlations to their production in the constituent quark level. If the applicability of the quark combination mechanism can be regarded as a judgment of QGP creation, then our results imply that the threshold for the onset of deconfinement is located in the energy region 11.6–20 A GeV, which is consistent with the report of the NA49 collaboration.

The authors would like to thank professor XIE Qu-Bing for fruitful discussions.

References

1 Adams J et al. (STAR collaboration). Nucl. Phys. A, 2005, **757**: 102
2 Adcox K et al. (PHENIX collaboration). Nucl. Phys. A, 2005, **757**: 184
3 Arsene I et al. (BRAHMS collaboration). Nucl. Phys. A, 2005, **757**: 1
4 Back B B et al. (PHOBOS collaboration). Nucl. Phys. A, 2005, **757**: 28
5 Alt C et al. (NA49 collaboration). Phys. Rev. C, 2008, **77**: 024903
6 Adare A et al. (PHENIX collaboration). Phys. Rev. Lett., 2007, **98**: 162301
7 Adcox K et al. (PHENIX collaboration). Phys. Rev. Lett., 2002, **88**: 242301
8 Greco V, Ko C M, Lévai P. Phys. Rev. Lett., 2003, **90**: 202302
9 Fries R J, Müller B, Nonaka C, Bass S A. Phys. Rev. Lett., 2003, **90**: 202303
10 Dénes Molnár, Sergei A Voloshin. Phys. Rev. Lett., 2003, **91**: 092301
11 SONG J, SHAO F L, XIE Q B. Int. J. Mod. Phys. A, 2009, **24**: 1161
12 SHAO C E, SONG J, SHAO F L, XIE Q B. Phys. Rev. C, 2009, **80**: 014909
13 SHAO F L, XIE Q B, WANG Q. Phys. Rev. C, 2005, **71**: 044903
14 SHAO F L, YAO T, XIE Q B. Phys. Rev. C, 2007, **75**: 034904
15 YAO T, ZHOU W, XIE Q B. Phys. Rev. C, 2008, **78**: 064911
16 WANG Y F, SHAO F L, SONG J, WEI D M, XIE Q B. Chin. Phys. C (HEP & NP), 2008, **32**: 976
17 SONG J, LIANG Z T, LIU Y X, SHAO F L, WANG Q. Phys. Rev. C, 2010, **81**: 057901
18 HAN W, LI S Y, SHANG Y H, SHAO F L, YAO T. Phys. Rev. C, 2009, **80**: 035202
19 Bearden I G et al. (BRAHMS collaboration). Phys. Rev. Lett., 2004, **93**: 102301
20 Alt C et al. (NA49 collaboration). Presented at Critical Point and Onset of Deconfinement 4th International Workshop, 2007, PoSCPOD07, 024. arXiv: nucl-ex, 2007, 0709.3030v1
21 Afanasiev S V et al. (NA49 collaboration). Phys. Rev. C, 2002, **66**: 054902
22 Afanasiev S V et al. (NA49 collaboration). Phys. Lett. B, 2000, **491**: 59
23 Alt C et al. (NA49 collaboration). Phys. Rev. C, 2008, **78**: 034918
24 Mischke A (NA49 collaboration). Nucl. Phys. A, 2003, **715**: 453c
25 Alt C et al. (NA49 collaboration). Phys. Rev. C, 2008, **78**: 044907 and references therein
26 CHEN J H et al. Phys. Rev. C, 2008, **78**: 034907
27 Lacasse R et al. (E877 collaboration). Nucl. Phys. A, 1996, **610**: 153c
28 Ahle L et al. (E802 collaboration). Phys. Rev. C, 1999, **59**: 2173
29 Ahle L et al. (E802 collaboration). Phys. Rev. C, 1998, **58**: 3523
30 Ahle L et al. (E802 collaboration). Phys. Rev. C, 1998, **57**: R466
31 Albergo S et al. (E896 collaboration). Phys. Rev. Lett., 2002, **88**: 062301
32 Barrette J et al. (E877 collaboration). Phys. Rev. C, 2000, **63**: 014902